# Joint channel estimation and symbol detection for OTFS system using a two-stage algorithm

Rabah Ouchikh, Abdeldjalil Aissa El Bey, Thierry Chonavel, Mustapha Djeddou

# Joint channel estimation and symbol detection for OTFS system using a two-stage algorithm

Rabah Ouchikh
*Lab Télécommunications*
*Ecole Militaire Polytechnique*
Bordj El-Bahri, Algeria
ouchikh16rabah@gmail.com

Abdeldjalil Aïssa-El-Bey
*IMT Atlantique, Lab-STICC,*
*UMR CNRS 6285, F-29238,*
Brest, France
abdeldjalil.aissaelbey@imt-atlantique.fr

Thierry Chonavel
*IMT Atlantique, Lab-STICC,*
*UMR CNRS 6285, F-29238,*
Brest, France
thierry.chonavel@imt-atlantique.fr

Mustapha Djeddou
*Electronics Department*
*National Polytechnic School*
Algiers, Algeria
djeddou.mustapha@gmail.com

***Abstract*—In this paper, we address the challenging problem of high pilot overhead and peak-to-average power ratio (PAPR) in channel estimation in high-mobility scenarios for 5G and beyond. To improve the channel estimation accuracy and enhance the reliability of data detection, we propose a two-stage algorithm for channel estimation and symbol detection in OTFS systems. In the first stage, a coarse estimate of the channel is obtained, followed by interference cancellation. Then, data symbols are detected using a message-passing (MP) algorithm. In the second stage, detected data and pilot symbols are jointly used to accurately estimate the channel. Simulations show that our proposed scheme, namely contiguous embedded pilots (CEP), achieves a good trade-off between complexity and performance in terms of normalized mean square error (NMSE), bit error rate (BER), spectral efficiency, and PAPR when compared to embedded pilot (EP) and superimposed pilot (SP) designs.**

***Index Terms*—OTFS, channel estimation, data detection, high-mobility, time-varying channels, message-passing, two-stage**

## I. Introduction

Future mobile communication systems face the challenge of maintaining reliable communications in high-mobility environments. However, the commonly used Orthogonal Frequency Division Multiplexing (OFDM) modulation experiences degraded performance in such environments [1]. Orthogonal Time Frequency Space (OTFS) modulation, proposed in recent works such as [2] and [3], is designed to tackle this issue by handling time-varying channels. OTFS employs the Inverse Symplectic Finite Fourier Transform (ISFFT) to transform a doubly-selective wireless channel into an almost flat one in the Delay-Doppler (DD) domain. To ensure robust data transmission in an OTFS system, effective channel estimation and data detection algorithms are necessary.

Several channel estimation schemes for OTFS in the DD domain have been proposed, and they can be divided into three categories. The first one concerns conventional pilot-aided (CPA) schemes in which a superframe architecture is used: the first frame is used for channel estimation, and the subsequent frames are used for data detection [4], [5]. The second category of algorithms, called embedded pilots (EP), consists of channel estimation and data detection in the same frame [1], [6]–[15]. This is achieved by arranging pilots and data symbols in the same DD grid. In this category, guard intervals are placed between pilots and data symbols to avoid interference between them. The third category called superimposed pilots (SP) includes schemes that superimpose pilots and data symbols in the same locations in the DD domain [16]–[19]. This category requires high-performance iterative algorithms for efficient channel estimation and accurate data detection.

This paper addresses the challenging problem of high pilot overhead and peak-to-average power ratio (PAPR) in channel estimation for high-mobility scenarios. We propose a two-stage algorithm for channel estimation and symbol detection in OTFS systems. In the first stage, we obtain a coarse channel estimate and perform interference cancellation, followed by symbol detection using a message-passing (MP) algorithm. In the second stage, we use the detected data and pilot symbols jointly as pilots to achieve more accurate channel estimation and update symbol detection accordingly.

*Notations:* $\odot$ and $\otimes$ denote, respectively, the Hadamard product and the Kronecker product. The column vectorization of an $M \times N$ matrix into an $MN$ column vector is denoted by $\mathrm{vec}(.)$. The invectorization of an $MN$ column vector to an $M \times N$ matrix is denoted by $\mathrm{vec}^{-1}(.)$. $\mathcal{CN}(m, \sigma^2)$ is the circular complex Gaussian distribution with a mean $m$ and a variance $\sigma^2$. $\mathrm{diag}\{d_1, d_2, ..., d_N\}$ denotes an $N \times N$ diagonal matrix with diagonal entries $d_1, d_2, ..., d_N$. $\mathbb{E}\{.\}$ is the expectation operation. Finally, $\boldsymbol{I}_M$, $\boldsymbol{F}_n$, and $\boldsymbol{F}_n^H$ are the $M \times M$ identity matrix, the $n$-point DFT matrix, and the $n$-point IDFT matrix.

## II. System design and problem formulation

We consider a Single-Input Single-Output OTFS system. The DD grid is divided into $N$ symbols and $M$ subcarriers. $\Delta f$, $B = M\Delta f$, and $T_f = NT$ are the subcarrier spacing, bandwidth, and the frame duration. We also have $T\Delta f = 1$.

At the transmitter side, pilots and data symbols are arranged in the same DD frame, as shown in Fig 1a. The transmitted DD signal is given as

$$\boldsymbol{X} = \boldsymbol{X}_d + \boldsymbol{X}_p, \tag{1}$$

where $\boldsymbol{X}_p \in \mathbb{C}^{M \times N}$ is formed by pilots in the $[l_p - l_\tau, l_p + M_p - 1] \times [k_p - k_\nu - N_p, k_p + k_\nu + N_p]$ sub-grid and zeros elsewhere, and $\boldsymbol{X}_d \in \mathbb{C}^{M \times N}$ is formed by zeros in the $[l_p - l_\tau, l_p + M_p - 1] \times [k_p - k_\nu - N_p, k_p + k_\nu + N_p]$ sub-grid and contains data symbols elsewhere. Parameters $l_\tau$ and $k_\nu$ denote

the maximum delay tap and the maximum Doppler tap of the channel. $(k_p, l_p)$ are the coordinates of the central pilot. To obtain an accurate estimation of the channel, it is necessary to use pilot signals of sufficient size to cover the maximum delay and Doppler spread. Therefore, the values of $M_p$ and $N_p$ are carefully selected to strike a balance between estimation accuracy and spectral efficiency.

After that, $\boldsymbol{X}$ passes through an ISSFT and the Heisenberg transform to obtain the time-domain signal given as

$$\boldsymbol{s} = (\boldsymbol{F}_N^H \otimes \boldsymbol{I}_M)\boldsymbol{x}, \tag{2}$$

where $\boldsymbol{x} = \text{vec}(\boldsymbol{X})$. A cyclic prefix (CP) is added to $s(t)$ before transmission to avoid inter-symbol interference.

The signal $s(t)$ is transmitted over the sparse $P$-path DD time-varying channel with the following impulse response:

$$h(\tau, \nu) = \sum_{i=1}^{P} h_i \delta(\tau - \tau_i)\delta(\nu - \nu_i), \tag{3}$$

where $h_i$ is the complex gain, $\tau_i$ is the delay shift, and $\nu_i$ is the Doppler shift for the $i$-th path.

The received signal, after removing the CP, is given as

$$\boldsymbol{r} = \boldsymbol{H}\boldsymbol{s} + \boldsymbol{n}, \tag{4}$$

where $\boldsymbol{n} \sim \mathcal{CN}(0, \sigma^2)$ and $\boldsymbol{H} = \sum_{i=1}^{P} h_i \boldsymbol{\Pi}^{l_i} \boldsymbol{\Delta}^{k_i}$, with $\boldsymbol{\Pi}$ being the right shift permutation matrix and $\boldsymbol{\Delta} = \text{diag}\{\exp(j2\pi(0)/MN), ..., \exp(j2\pi(MN-1)/MN)\}$. $l_i = \tau_i M \Delta f$ and $k_i = \nu_i NT$ denote the delay and Doppler taps.

Then, the Wigner transform and the symplectic finite Fourier transform (SFFT) are applied to $\boldsymbol{r}$, yielding

$$\boldsymbol{y} = (\boldsymbol{F}_N \otimes \boldsymbol{I}_M)\boldsymbol{r}. \tag{5}$$

After substituting (2) and (4) into (5), the relationship between $\boldsymbol{y}$, $\boldsymbol{x}_d = \text{vec}(\boldsymbol{X}_d)$, and $\boldsymbol{x}_p = \text{vec}(\boldsymbol{X}_p)$ can be expressed as follows:

$$\boldsymbol{y} = \boldsymbol{H}_{\text{eff}}\boldsymbol{x} + \tilde{\boldsymbol{n}} = \boldsymbol{H}_{\text{eff}}\boldsymbol{x}_d + \boldsymbol{H}_{\text{eff}}\boldsymbol{x}_p + \tilde{\boldsymbol{n}}, \tag{6}$$

where $\boldsymbol{H}_{\text{eff}} = (\boldsymbol{F}_N \otimes \boldsymbol{I}_M)\boldsymbol{H}(\boldsymbol{F}_N^H \otimes \boldsymbol{I}_M)$, and $\tilde{\boldsymbol{n}} = (\boldsymbol{F}_N \otimes \boldsymbol{I}_M)\boldsymbol{n} \sim \mathcal{CN}(0, \sigma^2)$. Equation (6) can be rewritten as

$$\boldsymbol{y} = \boldsymbol{\Phi}_p \boldsymbol{h} + \boldsymbol{\Phi}_d \boldsymbol{h} + \tilde{\boldsymbol{n}}, \tag{7}$$

where $\boldsymbol{\Phi}_k = [\boldsymbol{\Psi}_1 \boldsymbol{x}_k, \boldsymbol{\Psi}_2 \boldsymbol{x}_k, ..., \boldsymbol{\Psi}_P \boldsymbol{x}_k] \in \mathbb{C}^{MN \times P}$, $k \in \{p, d\}$, and $\boldsymbol{\Psi}_i = (\boldsymbol{F}_N \otimes \boldsymbol{I}_M)(\boldsymbol{\Pi}^{l_i}\boldsymbol{\Delta}^{\boldsymbol{k_i}})(\boldsymbol{F}_N^H \otimes \boldsymbol{I}_M) \in \mathbb{C}^{MN \times MN}$. $\boldsymbol{h} = [h_1, h_2, ..., h_P]^T \in \mathbb{C}^{P \times 1}$ has zero mean and covariance matrix $\boldsymbol{C_h} = \mathbb{E}\{\boldsymbol{h}\boldsymbol{h}^H\} = \text{diag}\{\sigma_{h_1}^2, \sigma_{h_2}^2, ..., \sigma_{h_P}^2\}$.

In this context, the objective is to estimate the channel by identifying the channel support $(l_i, k_i)_{i=1:P}$ and the associated path parameters $(h_i, \tau_i, \nu_i)_{i=1:P}$. On the other hand, symbol detection involves determining the data vector $\boldsymbol{x}_d$ from (6).

## III. Proposed Algorithm

In this paper, to improve the channel estimation accuracy and enhance the reliability of data detection, we propose a two-stage algorithm for channel estimation and symbol detection.

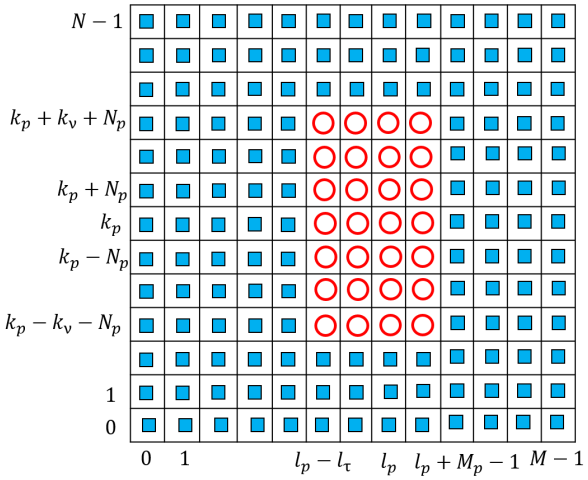


(a) Tx pattern.

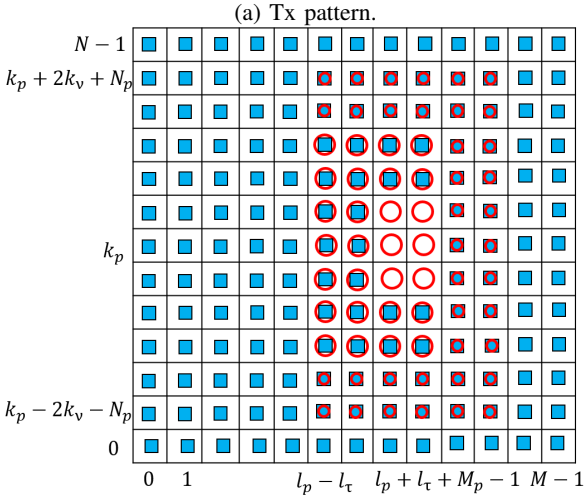


(b) Rx pattern.

Fig. 1: Tx and Rx patterns in the DD domain (○: pilot symbol, ■: data symbol).

### A. First stage

To estimate the channel, we use the $L_p = (2N_p + 1)M_p$ pilots uncontaminated by data symbols, as shown in Fig 1b. The received pilot vector $\boldsymbol{y}_p \in \mathbb{C}^{L_p \times 1}$ can be expressed as [6]

$$\boldsymbol{y}_p = (\boldsymbol{Z}_p \odot \boldsymbol{\Gamma})\tilde{\boldsymbol{h}} + \boldsymbol{v} = \boldsymbol{A}\tilde{\boldsymbol{h}} + \boldsymbol{v}, \tag{8}$$

where $\boldsymbol{Z}_p \in \mathbb{C}^{L_p \times L}$ represents the pilots matrix, $\boldsymbol{\Gamma}$ is an additional phase shift matrix, $L = (2k_\nu + 1)(l_\tau + 1)$, and $\tilde{\boldsymbol{h}}$ is a sparse vector containing only $P$ non-zero elements, which are the channel gains $\{h_i\}_{i=1:P}$.

To estimate the channel vector $\tilde{\boldsymbol{h}}$, we perform the Generalized Orthogonal Matching Pursuit algorithm (GOMP) [6] on (8). The positions of the non-zero entries of $\tilde{\boldsymbol{h}}$ correspond to delay and Doppler taps, and their values correspond to channel gains.

Once the channel is estimated, to detect data symbols, we first remove the contribution of pilots on the received signal (6) as

$$\boldsymbol{y}_d = \boldsymbol{y} - \hat{\boldsymbol{H}}_{\text{eff}}\boldsymbol{x}_p = \boldsymbol{H}_{\text{eff}}\boldsymbol{x}_d + \tilde{\boldsymbol{w}}, \tag{9}$$

where $\tilde{\boldsymbol{w}} = (\boldsymbol{H}_{\text{eff}} - \hat{\boldsymbol{H}}_{\text{eff}})\boldsymbol{x}_p + \tilde{\boldsymbol{n}}$ is the interference-plus-noise term. The detected data vector $\hat{\boldsymbol{x}}_d$ is obtained using the MP detector [16] with inputs $\tilde{\boldsymbol{h}}$, $\boldsymbol{y}_d$, $\mathbb{E}\{\tilde{\boldsymbol{w}}\}$, and $\mathbb{E}\{\tilde{\boldsymbol{w}}\tilde{\boldsymbol{w}}^H\}$.

An additional stage is required to achieve a precise channel estimate, which further enhances detection performance by reducing the interference term $(\boldsymbol{H}_{\text{eff}} - \hat{\boldsymbol{H}}_{\text{eff}})\boldsymbol{x}_p$.

### *B. Second stage*

To improve channel estimate and reduce detection errors, the pilot symbols and detected data from the first stage are utilized jointly as pilots in this second stage. This is accomplished by rewriting (7) as

$$\boldsymbol{y} = (\boldsymbol{\Phi}_p + \hat{\boldsymbol{\Phi}}_d)\boldsymbol{h} + (\boldsymbol{\Phi}_d - \hat{\boldsymbol{\Phi}}_d)\boldsymbol{h} + \tilde{\boldsymbol{n}} = \hat{\boldsymbol{\Phi}}\boldsymbol{h} + \tilde{\boldsymbol{v}}, \tag{10}$$

where $\hat{\boldsymbol{\Phi}} = \boldsymbol{\Phi}_p + \hat{\boldsymbol{\Phi}}_d$ is the joint pilot.

This method differs from the first stage in that it exploits all the entries of the received signal to estimate the channel, even those affected by data interference. By applying a Low-complexity Minimum Mean Square Error (LMMSE) estimator to (10), the channel vector is estimated as follows:

$$\hat{\boldsymbol{h}} = (\hat{\boldsymbol{\Phi}}^H\boldsymbol{C}_{\tilde{\boldsymbol{v}}}^{-1}\hat{\boldsymbol{\Phi}} + \boldsymbol{C}_{\boldsymbol{h}}^{-1})^{-1}\hat{\boldsymbol{\Phi}}^H\boldsymbol{C}_{\tilde{\boldsymbol{v}}}^{-1}\boldsymbol{y}, \tag{11}$$

where $\boldsymbol{C}_{\tilde{\boldsymbol{v}}} = \mathbb{E}\{\tilde{\boldsymbol{v}}\tilde{\boldsymbol{v}}^H\}$. Note that this estimator exploits the DD sparsity by computing the inverse of a $(P \times P)$ matrix, where $P \ll MN$.

Finally, to detect the data, we eliminate pilot contamination from the received signal using (9) and utilize the MP detector to detect the data matrix $\boldsymbol{X}_d$. Due to the more precise estimation of the channel vector in the second stage, the MP detector exhibits superior performance compared to that of the first stage.

## IV. Complexity analysis

Here, we will compare the computational complexity of CEP against that of the EP and SP schemes. All three schemes use the MP algorithm for data detection, and its overall cost over $n_{iter}$ iterations is denoted as $\mu_d = n_{iter}NMP|\mathcal{A}|$.

The computational complexity of the proposed algorithm is written as $C_{\text{CEP}} = \mathcal{O}(\mu_1)+\mathcal{O}(\mu_2)$, where $\mu_1$ and $\mu_2$ denote the computational cost of the first and second stage, respectively. $\mu_1 = \mu_e^{(1)} + \mu_d$ and $\mu_2 = \mu_e^{(2)} + \mu_d$, where $\mu_e^{(1)}$ and $\mu_e^{(2)}$ are the computational costs of the channel estimation step in the first and second stages, respectively. In the first stage, the GOMP algorithm is used to estimate the channel, and its computational cost is dominated by $\mu_e^{(1)} = \mathcal{O}(n_g L^2)$, where $n_g$ is the number of iterations required for the convergence of the GOMP. For the channel estimation step in the second stage, an LMMSE estimator is used, and its computational cost is dominated by $\mu_e^{(2)} = P^3$. Therefore, the computational complexity of the proposed algorithm is given as $C_{\text{CEP}} = \mathcal{O}(n_g L^2) + \mathcal{O}(P^3) + 2\mathcal{O}(n_{iter}NMP|\mathcal{A}|)$.

The overall complexity of the EP algorithm is dominated by $C_{\text{EP}} = \mathcal{O}(Nl_\tau) + \mathcal{O}(\mu_d)$, and the overall complexity of the SP algorithm is $C_{\text{SP}} = \mathcal{O}(\mu_e) + \mathcal{O}(\mu_d) + \mathcal{O}(\mu_i)$, where $\mu_i = \mu_e = (4P^2 + 6L)MN + (P^3 + L)$.

In practice, we have $P, L, l_\tau \ll MN$, so the overall complexities of CEP, EP, and SP algorithms are dominated by $C_{\text{CEP}} = 2\mathcal{O}(n_{iter}NMP|\mathcal{A}|)$, $C_{\text{EP}} = \mathcal{O}(n_{iter}NMP|\mathcal{A}|)$, and $C_{\text{SP}} = (n_s + 1)\mathcal{O}(MN) + n_s\mathcal{O}(n_{iter}NMP|\mathcal{A}|)$.

Finally, we can conclude that $C_{\text{EP}} < C_{\text{CEP}} < C_{\text{SP}}$. The proposed algorithm achieves a good balance between complexity and performance, making it a favourable choice in practical implementations.

## V. Simulation results

The performance of CEP is evaluated and compared to the EP scheme [1] and SP design [17] in terms of NMSE, BER, PAPR and spectral efficiency (SE).

We consider the following simulation parameters: the carrier frequency and the spacing between sub-carriers are given as $f_c = 4$ GHz and $\Delta f = 15$ kHz. Both the number of sub-carriers and symbols are set to $N = M = 64$. The Extended Vehicular A (EVA) channel model is employed [20], which features a maximum delay shift of $\tau_{max} = 20.8\ \mu s$, equivalent to a maximum delay tap of $l_\tau = 20$. Additionally, the model exhibits a maximum Doppler shift of $\nu_{max} = 1850$ Hz, indicating a high-mobility scenario with a maximum Doppler tap of $k_\nu = 8$ and a maximum speed of $v_{max} = 500$ km/h.

The total power in each OTFS frame is $MN$. Maintaining a constant total power for all schemes is essential for a fair comparison. In the EP scheme [1], due to the insertion of $(4k_\nu + 1)(2l_\tau + 1) - 1$ guard intervals (GI) between the pilot and data symbols, the power assigned to the GI positions must be reassigned to the pilot symbols. Thus, the EP scheme uses a pilot amplitude of $\sqrt{(4k_\nu + 1)(2l_\tau + 1)}$ to ensure that the total power in each OTFS frame remains constant. On the other hand, for the superimposed scheme [17], the power per DD symbol is 1 for $k \in [0, N-1]$ and $l \in [0, M-1]$. In this scheme, $30\%$ of the total power is allocated to pilots, and the remaining $70\%$ is allocated to data symbols.

Fig 2 presents the NMSE versus SNR performance for CEP, EP, and SP schemes. The results show that the proposed algorithm initially falls short of both the EP and SP schemes in the first stage, especially at low SNR levels. However, in the second stage, the channel estimation error of the proposed algorithm is significantly lower than those of both EP and SP, particularly at high SNR levels. The improvement in the second stage of the proposed algorithm is attributed to the joint utilization of pilot symbols and detected data for channel estimation. This enables more accurate channel estimation and reduction of the interference term, leading to superior performance compared to the first stage. On the other hand, in low SNR scenarios, the NMSE of the second stage is worse than EP. This can be attributed to the inadequate data detection caused by the poor channel estimation in the first stage of the proposed algorithm. However, at higher SNR levels, the benefits of the second stage's improved channel estimation

outweigh the limitations in the first stage, leading to overall better performance compared to EP and SP.

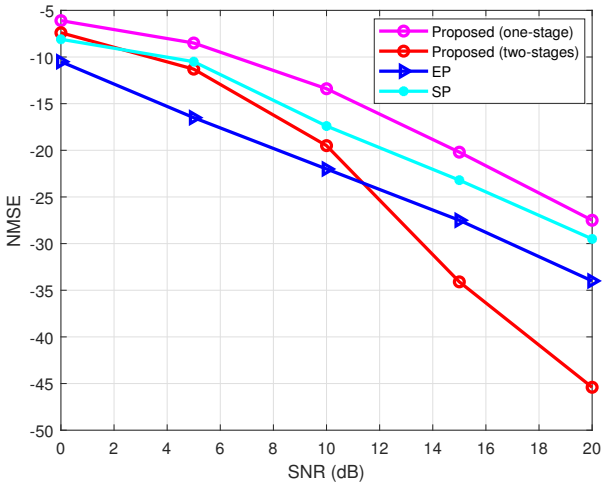


Fig. 2: NMSE of CEP, EP, and SP schemes.

In Fig. 3, the BER performance versus SNR is depicted. It shows that the BER of the second stage of CEP exceeds that of the SP scheme and matches that of the EP and known CSI. This indicates that the second stage of the proposed algorithm achieves comparable data detection performance to the EP and known channel state information (CSI) at higher SNR levels. Interestingly, the results also show that there is no need to consider further iterations of the process described in Section III. This means that the proposed two-stage algorithm provides satisfactory performance without requiring additional complexity and iterations. Furthermore, despite not achieving the same NMSE as the SP scheme, the first stage of CEP yields a BER that is close to the performance of the SP scheme. This suggests that the first stage's coarse channel estimation and interference cancellation steps are effective in improving data detection performance, even though the NMSE may be higher than SP.

We know investigate the PAPR performance for CEP, EP, and SP schemes. The EP design uses a pilot amplitude of $\sqrt{(4k_\nu+1)(2l_\tau+1)}$, and since CEP utilizes less pilot overhead (no guard intervals between pilots and data symbols and fewer pilots compared to EP), the dedicated pilot power per symbol in CEP is lower than that of EP. As the values of $M$ and $N$ increase, the channel parameters $l_\tau$ and $k_\nu$ also increase, leading to a rise in the power dedicated to a single pilot in the EP scheme, and consequently, a high PAPR. However, in the proposed scheme, the pilots are distributed in the DD domain, resulting in a low PAPR that changes only slightly with the increase of $M$ and $N$. To further confirm this result, the PAPR in dB for CEP, EP, and SP schemes is plotted as a function of $N$ in Fig. 4. From this figure, it can be observed that the PAPR of the EP method is significantly larger compared to those of CEP and SP schemes, which exhibit similar PAPR performance. Additionally, it is evident

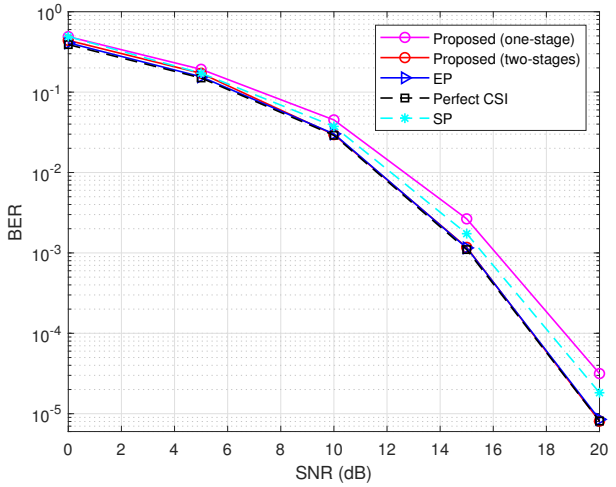


Fig. 3: BER performance of CEP, EP, and SP schemes.

that the PAPR of the EP scheme increases almost linearly with the increase in $N$, while the proposed scheme's PAPR changes only slightly with the increase in $N$. In summary, CEP demonstrates similar PAPR performance compared to SP and exhibits much lower PAPR compared to EP. At $N = 64$, there is about a 6 dB difference between CEP and EP schemes, and at $N = 512$, this difference increases to about 13 dB. This is attributed to the fact that the EP scheme uses only one high-power single pulse in the DD domain, while CEP distributes the pilots in the DD domain, leading to a more efficient power allocation and lower PAPR.

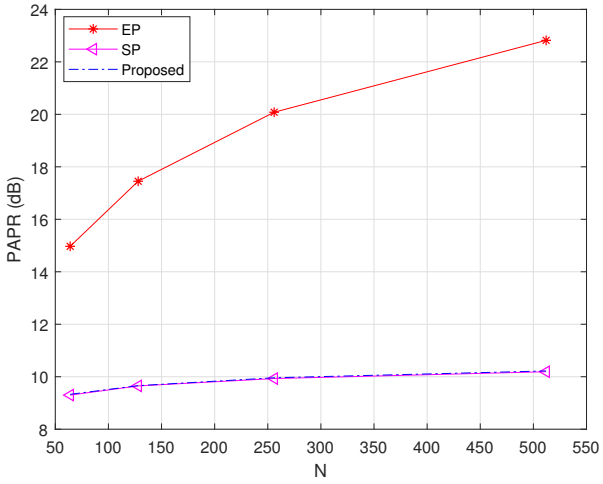


Fig. 4: PAPR of CEP, EP, and SP schemes.

The SE of CEP, EP, and SP schemes can be expressed as $SE = (1-\eta_s)\log_2(|\mathcal{A}|)$, where $\eta_s$ is the pilot overhead of scheme $s$ with $s \in$ Proposed, EP, SP and $\mathcal{A}$ is the constellation set. The pilot overhead is defined as the ratio of pilots-plus-GI to the total number of symbols in the OTFS frame: $\eta_{\text{EP}} = \frac{(4k_\nu+1)(2l_\tau+1)}{MN}$, $\eta_{\text{Proposed}} = \frac{(2N_p+1)M_p}{MN}$, and $\eta_{\text{SP}} = 0$.

Using the same constellation for CEP, EP, and SP schemes, the scheme with the least pilot overhead is the one with the best SE. As CEP uses less pilot overhead compared to EP, it achieves higher SE compared to EP. Therefore, CEP outperforms the EP design in terms of SE. To confirm this result, the SE of CEP, EP, and SP schemes for QPSK constellation and different $N$ and $M$ is plotted in Fig. 5. From the figure, it can be observed that CEP indeed outperforms the EP design in terms of SE and approaches the performance of the SP scheme for high values of $N$ and $M$. In summary, CEP achieves higher SE than the EP design due to its lower pilot overhead, and it converges to the performance of the SP scheme for higher values of $N$ and $M$. This indicates that the proposed algorithm strikes a good balance between pilot overhead and SE, making it a promising solution for future mobile communication systems.

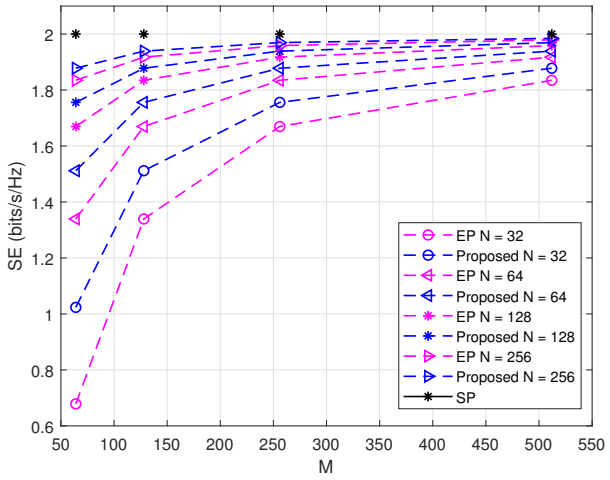


Fig. 5: SE performance of CEP, EP, and SP schemes for $|\mathcal{A}| = 4$.

## VI. Conclusion

In this paper, we have presented a novel two-stage approach for joint channel estimation and data detection in OTFS systems. The first stage utilizes the GOMP algorithm for coarse channel estimation based on pilots contribution not contaminated by data symbols and the MP algorithm for data detection. In the second stage, we take advantage of the detected data and pilot symbols to achieve accurate channel estimation. This approach offers significant improvements in both spectral and power efficiency while maintaining a low PAPR of the transmitter. Simulation results demonstrate that the proposed algorithm achieves a favorable trade-off between complexity and performance when compared to the conventional EP and SP schemes. The algorithm performs well in terms of NMSE, BER, PAPR, and SE. It shows promise as a practical solution for future mobile communication systems. Overall, the proposed two-stage approach shows considerable advantages over existing schemes, making it a compelling option for OTFS systems in high-mobility environments.

## References


[1] P. Raviteja, K. T. Phan, and Y. Hong, "Embedded pilot-aided channel estimation for OTFS in delay–doppler channels," *IEEE transactions on vehicular technology*, vol. 68, no. 5, pp. 4906–4917, 2019.

[2] A. Monk, R. Hadani, M. Tsatsanis, and S. Rakib, "OTFS-orthogonal time frequency space," *arXiv preprint arXiv:1608.02993*, 2016.

[3] R. Hadani, S. Rakib, M. Tsatsanis, A. Monk, A. J. Goldsmith, A. F. Molisch, and R. Calderbank, "Orthogonal time frequency space modulation," in *2017 IEEE Wireless Communications and Networking Conference (WCNC)*, pp. 1–6.

[4] I. A. Khan and S. K. Mohammed, "Low complexity channel estimation for OTFS modulation with fractional delay and doppler," *arXiv preprint arXiv:2111.06009*, 2021.

[5] F. Gómez-Cuba, "Compressed sensing channel estimation for OTFS modulation in non-integer delay-doppler domain," *arXiv preprint arXiv:2111.12382*, 2021.

[6] R. Ouchikh, A. Aïssa-El-Bey, T. Chonavel, and M. Djeddou, "Sparse channel estimation algorithms for OTFS system," *IET Communications*, vol. 16, no. 18, pp. 2158–2170, 2022.

[7] D. Shi, W. Wang, L. You, X. Song, Y. Hong, X. Gao, and G. Fettweis, "Deterministic pilot design and channel estimation for downlink massive MIMO-OTFS systems in presence of the fractional doppler," *IEEE Transactions on Wireless Communications*, vol. 20, no. 11, pp. 7151–7165, 2021.

[8] T. Li, C. Han, R. Yao, Y. Fan, and X. Zuo, "Low pilot overhead channel estimation for CP-OFDM-based massive MIMO OTFS system," *IET Communications*, vol. 16, no. 10, pp. 1071–1082, 2022.

[9] S. Srivastava, R. K. Singh, A. K. Jagannatham, and L. Hanzo, "Bayesian learning aided simultaneous row and group sparse channel estimation in orthogonal time frequency space modulated MIMO systems," *IEEE Transactions on Communications*, vol. 70, no. 1, pp. 635–648, 2021.

[10] L. Zhao, J. Yang, Y. Liu, and W. Guo, "Block sparse bayesian learning-based channel estimation for MIMO-OTFS systems," *IEEE Communications Letters*, vol. 26, no. 4, pp. 892–896, 2022.

[11] Y. Liu, Y. L. Guan, and D. González, "Near-optimal BEM OTFS receiver with low pilot overhead for high-mobility communications," *IEEE Transactions on Communications*, vol. 70, no. 5, pp. 3392–3406, 2022.

[12] F. Zhang, W. Ji, and L. Qiu, "Channel estimation for massive MIMO-OTFS systems via sparse bayesian learning with 2-D local beta process," in *2022 IEEE Wireless Communications and Networking Conference (WCNC)*. IEEE, 2022, pp. 1383–1388.

[13] R. Muzavazi and O. O. Oyerinde, "Channel estimation and data detection schemes for orthogonal time frequency space massive MIMO systems," *Computers and Electrical Engineering*, vol. 102, p. 108215, 2022.

[14] R. Mallaiah, K. Vejandla, V. Mani, A. Kumar, and M. Sellathurai, "An embedded pilot power based channel estimation and low-complexity feedback equalization scheme for OTFS system," *Physical Communication*, vol. 55, p. 101875, 2022.

[15] M. Li, S. Zhang, Y. Ge, F. Gao, and P. Fan, "Joint channel estimation and data detection for hybrid RIS aided millimeter wave OTFS systems," *IEEE Transactions on Communications*, vol. 70, no. 10, pp. 6832–6848, 2022.

[16] H. B. Mishra, P. Singh, A. K. Prasad, and R. Budhiraja, "Iterative channel estimation and data detection in otfs using superimposed pilots," in *2021 IEEE International Conference on Communications Workshops (ICC Workshops)*, pp. 1–6.

[17] R. Ouchikh, A. Aïssa-El-Bey, T. Chonavel, and M. Djeddou, "Iterative channel estimation and data detection algorithm for OTFS modulation," in *2022 IEEE International Conference on Acoustics, Speech and Signal Processing (ICASSP)*, pp. 5263–5267.

[18] ——, "Alternative threshold-based channel estimation and message-passing-based symbol detection in mimo-otfs systems using superimposed pilots," *Physical Communication*, vol. 59, p. 102091, 2023.

[19] R. Ouchikh, T. Chonavel, A. A. El Bey, and M. Djeddou, "Joint channel estimation and data detection for high rate OTFS systems," *International Journal of Communication Systems*, 2023.

[20] U. E. U. conformance specification Radio, "3rd generation partnership project; technical specification group radio access network; evolved universal terrestrial radio access (E-UTRA); user equipment (UE) conformance specification radio transmission and reception," 2011.